Visual Neuroscience (2005), **22**, 721–734. Printed in the USA.

DOI: 10.1017/S0952523805226044

Morphological characterization of the retinal degeneration in three strains of mice carrying the *rd-3* mutation

KENNETH A. LINBERG,[1] ROBERT N. FARISS,[1] JOHN R. HECKENLIVELY,[3,5] DEBORA B. FARBER,[3,4] AND STEVEN K. FISHER[1,2]

[1]Neuroscience Research Institute, University of California, Santa Barbara, California
[2]Department of Molecular, Cellular and Developmental Biology, University of California, Santa Barbara, California
[3]The Jules Stein Eye Institute, Los Angeles, California
[4]The Molecular Biology Institute, UCLA, Los Angeles, California
[5]Harbor-UCLA Medical Center, Torrance, California

(RECEIVED November 17, 2004; ACCEPTED April 25, 2005)

Abstract

Retinal development in 3 strains of *rd-3/rd-3* mutant mice, previously shown to have different rates of degeneration, was studied using light, electron, and immunofluorescence microscopy. The time course and phenotype of the degeneration as well as details on the mechanism of massive photoreceptor cell loss are compared with other known retinal degenerations in mice. Up until postnatal day (P) 10, the retinas of all three strains (RBF, 4Bnr, In-30) develop similarly to those of pigmented and nonpigmented controls. TUNEL-positive cells appear in the outer nuclear layer (ONL) by P14, and reach a maximum in all three mutant strains around P21. Scattered rods and cones form a loose, monolayered ONL by 8 weeks in the albino RBF strain, by 10 weeks in the albino 4Bnr strain, and by 16 weeks in the pigmented In-30 strain. Though the initial degeneration begins in the central retina, there is no preferred gradient of cell death between central and peripheral photoreceptors. Rods and cones are present at all ages examined. During development, stacks of outer segments (OS) form in all three strains though they never achieve full adult lengths, and often have disorganized, atypical OS. Rod opsin is expressed in the developing OS but is redistributed into plasma membrane as OS degeneration proceeds. Retinal pigment epithelial (RPE) cells of all mutant strains contain packets of phagocytosed OS, and their apical processes associate with the distal ends of the OS. At their synaptic sites, photoreceptor terminals contain ribbons apposed to apparently normal postsynaptic triads. As photoreceptors are lost, Müller cells fill in space in the ONL but they do not appear to undergo significant hypertrophy or migration, though during the degeneration, glial fibrillary acidic protein (GFAP) expression is gradually upregulated. Macrophage-like cells are found frequently in the subretinal space after the onset of photoreceptor apoptosis. As OS disappear, the RPE apical processes revert to simple microvilli. Late in the degeneration, some RPE cells die and neighboring cells appear to flatten as if to maintain confluence. In regions of RPE cell loss that happen to lie above retina where the ONL is gone, cells of the inner nuclear layer (INL), wrapped by Müller cell processes, may front directly on Bruch's membrane.

Keywords: Inherited retinal degeneration, Apoptosis, Photoreceptors

Introduction

The *rd-3* retinal degeneration (Heckenlively et al., 1993*a*,*b*; Chang et al., 1993*a*; Roderick et al., 1995) is a murine hereditary retinal disorder that may provide an additional model for understanding human inherited retinal degenerations. It is caused by an autosomal recessive gene on chromosome 1, at a totally different locus than the genes associated with the *rd* (Carter-Dawson et al., 1978), *Rds* (Sanyal et al., 1980), *pcd*, *nr* (Mullen & LaVail, 1975), *mnd* (Chang et al., 1994), *tubby* (Heckenlively et al., 1995), $mitf^{vit}$ (vitiligo; Lamoreux et al., 1992), *rd6* (Hawes et al., 2000), $Cr1^{rd8}$ (Mehalow et al., 2003), or $Rpe65^{rd12}$ (Pang et al., 2005) degenerations in mice. Crossbreeding of *rd-3/rd-3* mice with mice homozygous for the first six of these mutations produce unaffected offspring (Chang et al., 1993*a*, 1994; Heckenlively et al., 1995).

Preliminary studies using both morphological and electroretinogram (ERG) data showed a strong correlation between the time course of photoreceptor loss in each strain and the gradual extinction of the *a*-wave in each (Chang et al., 1993*a*; Heckenlively et al., 1993*b*; Nusinowitz et al., 1997). These results indicated that

Address correspondence and reprint requests to: Steven K. Fisher, Neuroscience Research Institute, University of California Santa Barbara, Santa Barbara, CA 93106-5060, USA. E-mail: fisher@lifesci.ucsb.edu

Current Address of Robert N. Fariss: Biological Imaging Core, NEI-NIH, Bethesda, MD 20892-0703, USA.

Current Address of John R. Heckenlively: Ophthalmology, University of Michigan, Ann Arbor, MI 48105, USA.

the time course of the *rd-3* rod/cone degeneration is of intermediate duration when compared to other retinal degenerations in mice (Carter-Dawson et al., 1978; Messer et al., 1993; Mullen & LaVail, 1975; Sanyal et al., 1980). Photoreceptor degeneration begins at the time of outer segment differentiation, reaching completion in 2–4 months. Furthermore, the rate of degeneration appears to depend upon the strain of mice carrying the mutation, since Heckenlively et al. (1993*a*,*b*) showed that the rate of degeneration was more rapid in two albino strains {RBF/DnJ or RBF, Rb(11.13)Bnr or 4Bnr} than in a pigmented strain {In(5)30Rk or In-30}. In order to better determine if this is an example of a mutation that is differentially expressed depending upon the genetic background of the organism, we have further detailed the development and degeneration of the retina in these same three strains and compared them to pigmented (C57BL/6J) and albino (BALB/cJ) normal mice using light, electron, and immunofluorescence confocal microscopy. We used the TUNEL technique (Gavrieli et al., 1992) to study the time course of apoptotic cell death in the *rd-3* mutants since this is the primary mechanism of photoreceptor loss in other inherited retinal degenerative diseases (Chang et al., 1993*b*; Lolley et al., 1994; Portera-Cailliau et al., 1994; Smith et al., 1995; Ikeda et al., 1999; Guarneri et al., 2004).

Portions of this report have appeared elsewhere in abstract form (Linberg et al., 1994; Fariss et al., 1994).

Materials and methods

In addition to pigmented (C57BL/6J) and albino (BALB/cJ) control mice ($n = 8$), animals of the three strains homozygous for the *rd-3* mutation [(RBF/DnJ(RBF) ($n = 15$), Rb(11.13)Bnr(Bnr) ($n = 17$), and In(5)30Rk(In-30) ($n = 18$)] were used in this study. Housed at the Jackson Laboratory, Bar Harbor, ME, the Jules Stein Eye Institute, UCLA, and the Harbor-UCLA Medical Center, all mice were maintained on a 12-h light/12-h dark lighting regimen using normal vivarium room lighting. All procedures and protocols conformed to NIH guidelines and were approved by the appropriate University committees on animal use. At specified postnatal time points between 6 days and 17 weeks, animals were euthanized by lethal injection of Avitene. They were perfused with fixative by intracardial injection, eyes were enucleated, and an incision was made across the cornea or near the limbus to facilitate penetration of fixative.

Animals homozygous for the strains listed above will be referred to in the text as RBF, 4Bnr, and In-30, respectively.

Light and electron microscopy

For light and electron microscopy, the retinas were fixed, dehydrated, and embedded as described elsewhere (Fisher et al., 1993).

Tissue sections, 0.5 μm thick, that extend through the optic nerve head and include retinal tissue to the ora serrata on either side, were used to obtain comparative retinal measurements by light microscopy. The toluidine blue-stained sections were divided into six regions of approximately equal arc (2 central regions on either side of the optic nerve, 2 midperipheral, and 2 peripheral) in which the thicknesses of retinal layers were measured and the number of pyknotic profiles counted. [Pyknotic nuclei in this type of preparation have typically been equated with cells undergoing apoptosis (Young, 1984).] We did not compare inferior *versus* superior or nasal *versus* temporal regions of the retinas studied, but we carefully compared central to peripheral regions of the retinas and never found significant differences in cell counts or thicknesses of retinal layers between them.

An Olympus BX60 microscope was used for light microscopy (LM) and a Philips CM-10 for electron microscopy (EM).

Fig. 1. A: A light micrograph (LM) of midperipheral retina, P3, RBF strain. Darkly staining cells comprise the broad outer neuroblast layer (ONbL). Lightly staining amacrine cells (brace) are just distal to the inner plexiform layer (IPL). Arrows = mitotic figures; arrowheads = apoptotic profiles; "*" = retinal pigmented epithelium (RPE). 265×. B: LM of central retina, P5, RBF strain. Amacrine cells (small brace) and 4–5 overlying rows of lightly staining outer neuroblasts (large brace) underlie the rest of the ONbL. Horizontal cells (HCs) (arrows) and an incipient outer plexiform layer (OPL) (arrowhead) begin to subdivide this thick layer. "*" = RPE. 360×. C: LM of central retina, P6, C57BL/6J control. Arrows indicate the developing but discontinuous OPL. Arrowhead = apoptotic profiles; brackets as in Fig. 1B. 275×. D: LM of midperipheral retina, P8, 4Bnr strain. A thin OPL subdivides the field of rod precursors at the inner margin of which lies an apoptotic cell (arrowhead). "*" = inner segments (IS); ONL = outer nuclear layer; INL = inner nuclear layer. 275×. E: LM of the normal midperipheral retina, P10, BALB/cJ control. Most rod precursors now lie above the OPL. Arrowheads = apoptotic cell bodies in the INL. IS (*) appear of similar length to those in Fig. 1D. 275×. F: LM of central retina, P11, In-30 strain. Photoreceptor cell bodies are restricted to the ONL. Arrowhead = apoptotic profile in the INL; is = inner segments. 275×. G: LM of central retina, P12, RBF strain. Darkly staining outer segments (OS) (arrow) lie above the receptor IS. 335×. H: LM of central retina, P14, BALB/cJ control. The OS (arrow), IS and ONL have similar thicknesses to those in Fig. 1G. olm = outer limiting membrane; bv = blood vessel; brace = amacrine cell layer. 335×. I: LM of central retina, P14, 4Bnr strain. A thick ONL contains several apoptotic profiles (arrowheads); one lies below the OPL and may be a dying "inner" rod. A photoreceptor cell body lies in the subretinal space among the IS (arrow). The brace spans the height of the receptor OS. 380×. J: LM of midperipheral retina in a different P14, 4Bnr strain, whose narrow ONL has only 5–6 rows of photoreceptor nuclei. Except for one in the RPE, all apoptotic profiles lie in the ONL (arrowheads). A photoreceptor cell body lies in the subretinal space (arrow). IS and OS are much less distinguishable and shorter than those in Fig. 1I. 380×. K: An electron micrograph (EM) of the interface of retina and RPE in a P6 mouse, 4Bnr strain. A photoreceptor connecting cilium (ci) shows no OS. Arrow = basal body; mv = RPE apical microvilli; m = mitochondria; n = RPE cell nucleus. 14,500×. L: EM of developing OS in a P12 mouse, RBF strain. ci = connecting cilium. 22,500×. M: EM of developing OS in a P8 mouse, 4Bnr strain. is = inner segments; ci = connecting cilium. 9350×. N: EM of a synaptic ribbon (arrow) in the perinuclear cytoplasm of a rod terminal in a P8 mouse, 4Bnr strain. The postsynaptic process is electron-lucent and contains vesicles. n = rod nucleus. 28,000×. O: EM of a HC and the developing OPL, P8 mouse, 4Bnr strain. Rod precursors (*) lie among the HCs on the proximal edge of the OPL, but are not seen deeper in the INL. Processes of the OPL neuropil display a diversity of size and staining density. 3200×. Scale bars: A–J = 20 μm; K, M = 1 μm; L, N = 0.5 μm; O = 5 μm.

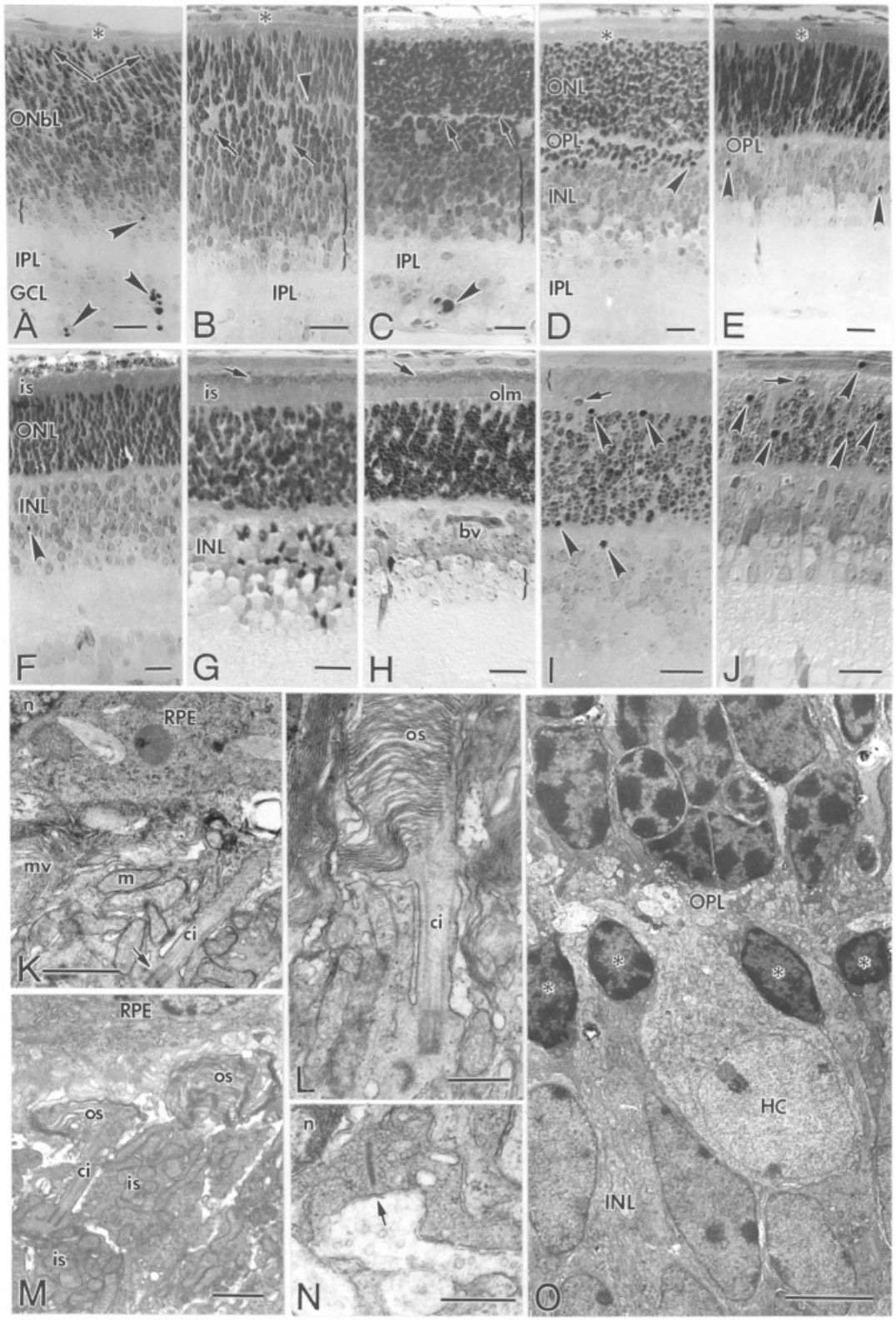
ONbL
IPL
GCL
A
IPL
B
IPL
C
ONL
OPL
INL
IPL
D
OPL
E
is
ONL
INL
F
is
INL
G
olm
bv
H
I
J
n
RPE
mv
m
ci
K
os
ci
L
OPL
HC
INL
RPE
os
os
ci
is
is
M
n
N
O

FIGURE 1

Immunocytochemistry

The techniques for immunocytochemistry were as described by Matsumoto and Hale (1993).

For this study, antibodies to glial fibrillary acidic protein (GFAP; Dako, Carpinteria, CA) and rod opsin (mouse anti-bovine opsin, monoclonal rho4D2; courtesy of Dr. Robert Molday) were applied to sections of retina for 15 h. After repeated buffer washes, sections were placed in the fluorescein-conjugated secondary antibody for 15 h and then washed again with buffer several times. Sections were mounted in glycerol containing n-propyl gallate and viewed using a Bio-Rad 500 laser scanning confocal microscope.

Fluorescent labeling of apoptotic cells using the TUNEL method

To identify apoptotic cells in the mouse retina, a TUNEL (TdT-mediated dUTP-biotin nick end labeling) method modified from Gavrieli et al. (1992) and Portera-Cailliau et al. (1994) was employed using 100-μm thick Vibratome sections of agarose-embedded retina. Fragmented DNA was labeled by incubating sections in a Tris buffer solution containing biotin 16-dUTP (Boehringer Mannheim, Germany) and terminal transferase (Boehringer Mannheim) at 37°C for 2 h, and the biotin labeling visualized *via* fluorescein-conjugated streptavidin. Sections were observed using a Bio-Rad 500 laser scanning confocal microscope.

Results

Developmental sequence: Postnatal week one (Birth to P6)

As illustrated for the RBF strain, at postnatal day (P) 3 the outer retina consists of a densely staining, thick outer neuroblast layer (ONbL) overlying 2–3 rows of developing amacrine cells (Fig. 1A). A thin inner plexiform layer (IPL) is interposed between the outer retina and the ganglion cell layer (GCL). Mitotic figures at the interface of the retina with the RPE are still found in the mid-periphery (Fig. 1A, arrows). Pyknotic profiles of cells undergoing apoptosis are restricted to the GCL (Figs. 1A & 1C) and the innermost rows of the ONbL (Fig. 1A). The outermost cells of this layer, which will become photoreceptors, have yet to develop outer segments (OS). This lack of OS persists centrally at least until P6 (Fig. 1K), and peripherally, even longer.

By P5 developing horizontal cells (HCs) are evident in the central retina of both control and all three strains of *rd-3* mice (Fig. 1B). The outer plexiform layer (OPL) is forming but is discontinuous until the end of the first postnatal week (Fig. 1C). In all strains, roughly two-thirds of the photoreceptor precursors, the "outer" rods, lie distal to the developing OPL, while one-third, the "inner" rods (Young, 1984), are proximal to it (Figs. 1B & 1C). Pyknotic profiles occur only in the developing inner nuclear layer (INL) and the GCL (Fig. 1C) (see Tables 1–4). EM shows the occurrence of synaptic structures in the developing photoreceptor terminals of both the normal and mutant mice (Fig. 1N).

At the end of the first postnatal week, the combined thickness of the inner segment (IS) and OS layers for all strains of *rd-3/rd-3* and control mice measured 7–9 μm (see Tables 1–4).

Developmental sequence: Postnatal week two (P7 to P13)

During the first part of the second postnatal week, the OPL continues to thicken while the number of "inner rods" decreases so that by P8 they form only a discontinuous row at the posterior retinal pole (Figs. 1D & 1O). Posteriorally, OS are first seen by EM at this time (Fig. 1M). At P8–P11, the ONL consists of 10–12 rows of nuclei (Figs. 1E & 1F), the combined length of the IS and OS averages 10–12 μm. The greatest number of apoptotic profiles still occurs deep in the INL (Figs. 1E & 1F) (4 to 7/mm in all three strains of *rd-3* mice and controls; see Tables 1–4), with increasing numbers at the outer border of the OPL (Figs. 1I & 2H) or among the "inner" rods and HCs (Figs. 1D & 1I). EM reveals the presence of a true OPL neuropil (Fig. 1O) that contains a variety of processes including some postsynaptic to rod ribbons (Fig. 1N).

During the last half of the second postnatal week, the rod OS can be distinguished from the IS by LM (Figs. 1G, 1H, & 1I). The pigmented and albino controls and the pigmented In-30 strain develop their OS 1–2 days before the RBF (Fig. 1L) and 4Bnr (Fig. 1M) strains. All three mutant strains develop OS that in some cells appear normal (Olney, 1968) (Fig. 1L), while in others are clearly

Table 1. *RBF strain*

Age (days)	Thickness: OS + IS (μm)	Thickness: ONL (μm)	ONL: # apo/mm*	Thickness: INL (μm)	INL: apo/mm*	GCL: apo/mm*
3	—	—	1.3	—	4.4	1.6
5	7.3	82.0	0.5	56.0	4.6	2.1
7	5.5	49.0	0.0	60.0	4.7	0.0
7	5.3	55.0	0.5	67.0	8.4	0.5
10	17.3	58.0	0.4	60.0	4.0	0.2
12	18.2	60.0	1.1	57.0	1.9	0.3
14	25.8	46.0	8.5	58.0	2.4	0.0
14	17.3	60.0	8.0	59.0	1.4	0.0
17	33.7	48.0	13.2	51.0	0.7	0.0
21	18.6	25.0	20.5	44.0	0.5	0.0
28	7.4	13.0	11.6	33.0	0.0	0.0
42	5.5	11.0	12.8	31.0	1.0	0.0
54	0.0	6.0		38.0	0.0	0.8
56	0.0	4.2	10.1	49.0	1.1	0.0
76	0.0	4.0	2.4	34.0	1.4	0.0

*apo/mm = apoptotic profiles per millimeter of retina.

Table 2. *4Bnr strain*

Age (days)	Thickness: OS + IS (μm)	Thickness: ONL (μm)	ONL: # apo/mm*	Thickness: INL (μm)	INL: apo/mm*	GCL: apo/mm*
6	7.3	82.8	1.5	58.0	5.7	0.9
6	7.6	74.3	1.2	49.0	7.0	3.8
8	11.3	81.5	4.4	74.0	6.6	0.6
8	10.9	71.0	2.2	51.0	4.7	0.2
10	12.7	67.4	0.9	66.0	5.8	0.0
14	20.0	32.8	11.5	56.0	0.9	0.0
14	7.3	31.8	31.2	58.0	1.0	0.5
21	6.4	15.8	19.3	53.0	0.0	0.0
25	2.9	8.9	6.1	37.0	0.9	0.0
28	2.4	8.5	5.3	45.0	0.5	0.0
32	2.7	6.7	4.0	41.0	0.2	0.0
35	3.1	10.2	4.7	31.0	1.0	0.0
42	5.7	5.7	5.3	37.0	1.9	0.3
56	2.2	5.1	4.9	35.0	0.2	0.0
77	1.3	4.2	1.4	40.0	0.9	0.3
77	1.4	4.5	2.4	36.0	0.4	0.0
91	1.0	4.4	0.3	40.0	0.0	0.3

*apo/mm = apoptotic profiles per millimeter of retina.

Table 3. *In-30 strain*

Age (days)	Thickness: OS + IS (μm)	Thickness: ONL (μm)	ONL: # apo/mm*	Thickness: INL (μm)	INL: apo/mm*	GCL: apo/mm*
6	—	47.0	1.0	72.0	3.5	1.9
6	8.4	46.0	2.4	65.0	15.4	1.7
8	11.1	49.0	0.0	65.0	4.4	1.2
10	11.2	54.0	0.2	64.0	4.1	0.4
11	15.4	50.0	0.2	60.0	7.6	1.7
14	23.6	49.0	3.0		1.2	0.2
14	27.3	46.0	12.5	50.0	0.6	0.0
16	29.1	45.0	16.4	50.0	1.5	0.0
17	29.1	47.0	14.5	47.0	0.4	0.0
20	29.5	48.0	35.3	56.0	1.4	0.0
21	27.3	40.0	17.5	51.0	0.0	0.0
24	21.0	29.0	14.1	43.0	0.0	0.0
27	25.5	30.0	18.8	38.0	0.4	0.2
29	22.4	26.0	12.3	35.0	0.5	0.0
45	21.3	20.0	6.3	44.0	0.2	0.0
49	20.0	21.0	3.7	33.0	0.4	0.0
77	2.7	6.0	2.8	35.0	1.5	0.0
98	3.6	6.4	3.6	39.0	0.8	0.0

*apo/mm = apoptotic profiles per millimeter of retina.

Table 4. *Controls*

Age (days)	Thickness: OS + IS (μm)	Thickness: ONL (μm)	ONL: # apo/mm*	Thickness: INL (μm)	INL: apo/mm*	GCL: apo/mm*
6*	9.5	87.0	0.8	58.0	7.7	2.0
10	14.6	60.1		45.5		
14	19.1	82.0	0.7	56.0	0.8	0.5
14*	27.3	75.0	0.6	52.0	0.7	0.2
21	36.0	46.0	0.7	40.0	0.0	0.0
28*	45.5	58.2		52.8		
49	46.0		0.0	31.0	0.0	0.0
70*	65.5	51.0		47.3		

*Pigmented controls.

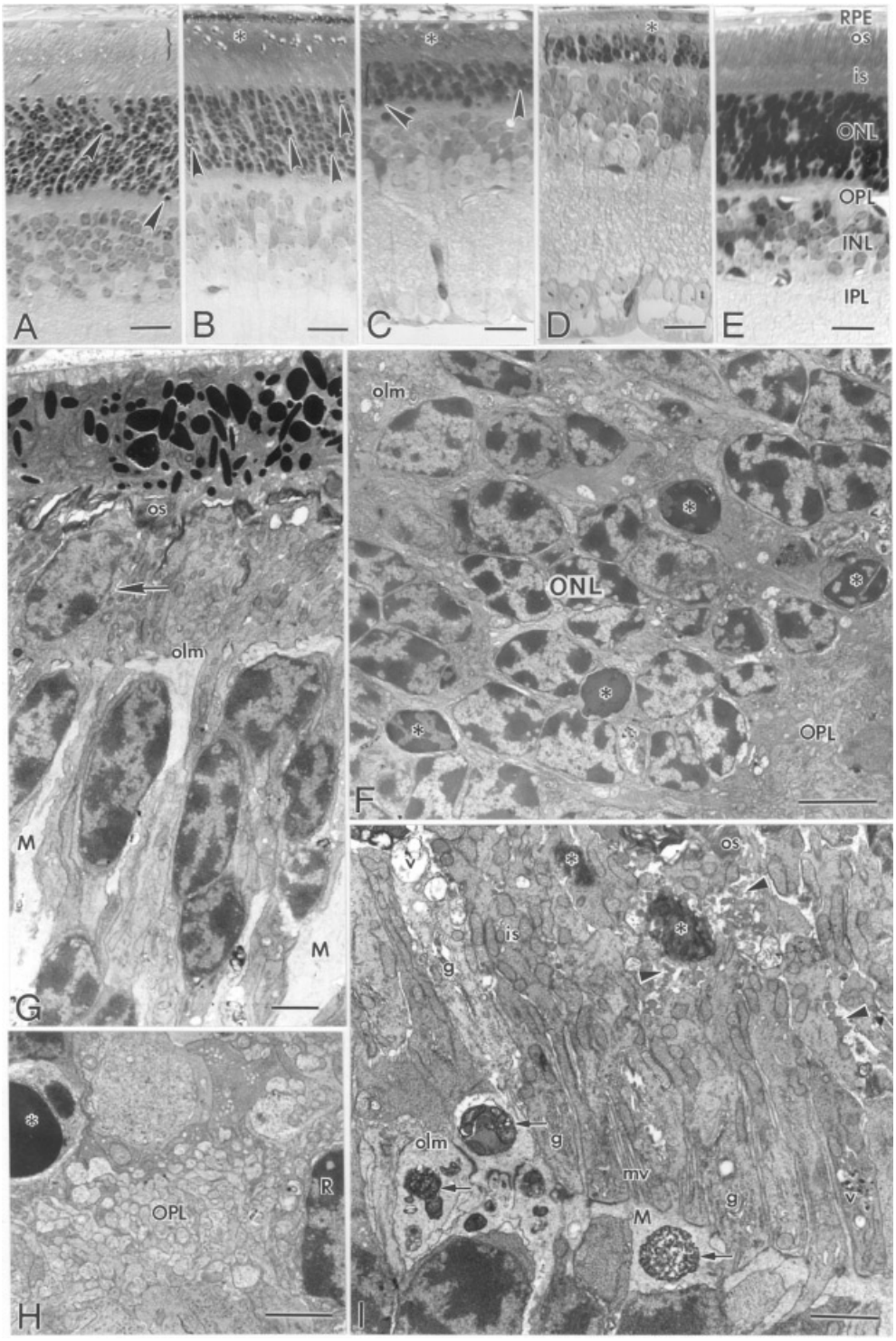

Fig. 2. A: LM of central retina, P17, RBF strain. A brace spans the OS layer. Arrowheads = apoptotic cell bodies in the ONL. 380×. B: LM of central retina, P20, In-30 strain. Arrowheads = apoptotic cells in the ONL. "*" = OS layer. 380×. C: LM of midperipheral retina, P21, RBF strain. A brace spans the ONL, only 4–5 rows thick, that contains apoptotic profiles (arrowheads). OS (*) are shorter than those in Fig. 2A. 380×. D: LM of central retina, P21, 4Bnr strain. A brace spans the ONL, only 2–3 rows thick. Most of the remaining photoreceptor cell bodies stain densely. Neither receptor OS nor IS are evident in the subretinal space (*). 380×. E: LM of midperipheral retina, P21, BALB/cJ control taken at the same magnification as the others for purposes of comparison. 380×. F: EM of the retina of a P14 mouse, 4Bnr strain. Four apoptotic cells (*) lie in the thin ONL. Note the OLM and the OPL. 2900×. G: EM of outer retina, P10 mouse, In-30 strain. Developing OS are abnormal. An ectopic photoreceptor cell body (arrow) lies among IS above the OLM. Müller cell cytoplasm (M) is electron-lucent and contains some electron-dense debris. 4200×. H: EM of the retina of a P10.5 mouse, 4Bnr strain. An "inner" rod (R) still lies proximal to the OPL neuropil. An apoptotic cell (*) lies among photoreceptor terminals. 6250×. I: EM of the retina of a P21 mouse, In-30 strain. Receptor outer segments in normal (os) and abnormal (*) arrays lie distal to the receptor IS. Some IS are vacuolated (v) and have unusual extracellular vesicles (arrowheads) between them. Lying mostly proximal to the OLM, electron-lucent Müller cell (M) cytoplasm contains electron-dense inclusions (arrows). mv = Müller cell apical microvilli; g = Golgi body. 6250×. Scale bars: A–E = 20 μm; F = 5 μm; G–I = 2 μm.

abnormal (Fig. 2G). Overall, by P14 the combined length of the IS and OS ranged from 20 μ to 30 μm in the controls, the RBF, and In-30 strains, but only 7–20 μm in the 4Bnr strain (see Tables 1–4). Phagosomes appear in the RPE of all specimens at this time, suggesting that there is no defect in the phagocytic process.

During the latter part of the second postnatal week, major abnormalities are first evident in all three strains of *rd-3/rd-3* mice. Apoptotic profiles appear among the differentiating photoreceptors (Figs. 1I, 1J, & 8A; Tables 1–3) which is not a developmentally normal occurrence for the emerging ONL (Fig. 8A; Table 4). In all three mutant strains, the numbers of ONL apoptotic profiles per millimeter of retina rise from under 1 at P10 to 8–12 at P14. In both controls they remained under 1/mm. Although there can be considerable variation between eyes from mice of the same age and strain, the rate of photoreceptor loss is greatest for the 4Bnr strain (see, for example, Fig. 2F), less for the RBF strain, and least, but still elevated, for the In-30 strain (see Figs. 8A & 8B).

Developmental sequence: Postnatal week three (P14 to P20)

Although the rate of photoreceptor loss varies among the *rd-3/rd-3* strains, the beginning of mass apoptosis in all three seems to arise concurrently during week 3 (see Figs. 8A & 8B; Tables 1–3). At the beginning of the week, the In-30 strain had 10 rows of photoreceptors in the central retina with an average number of apoptotic profiles close to 15/mm. By midweek the RBF strain had slightly fewer rows of rod nuclei with 13 apoptotic profiles/mm (Fig. 2A). By the end of the week, the In-30 strain (Fig. 2B) still had about 8 rows of photoreceptor nuclei (the control retinas at a similar age had 10–11 rows, see Fig. 2E) whereas the other two strains showed a much more dramatic loss of cells (RBF strain, Fig. 2C; 4Bnr strain, Figs. 2D & 2F). The number of apoptotic profiles for all three strains ranged from 17–21/mm of retina (Tables 1–3) while the P21 controls had none (Fig. 2E; Table 4). In the *rd-3* mice, the IS and OS never achieved normal length (see Fig. 8C; Tables 1–3). In one 4Bnr specimen, the IS/OS length reached only 6 μm; while OS were not discernible by LM (Fig. 2D), EM revealed abnormally thin, distorted, and elongated stacks of OS (Fig. 3H).

Concurrent with the dramatic increase in the rate of photoreceptor loss is the appearance of macrophages in the subretinal space (Figs. 3A, 4B, 4C, & 4H) that are believed to assist the RPE in scavaging and clearing cellular debris (Finnemann & Rodriguez-Boulan, 1999; Hisatomi et al., 2003).

Developmental sequence: Postnatal week four (P21 to P27)

In all three strains the ONL continues to lose cells, but the RBF and In-30 strains show over twice as many apoptotic profiles as the 4Bnr strain (see Figs. 8A–8B; Tables 1–3). This disparity reflects the fact that most photoreceptors have already died in the 4Bnr strain. By the end of the first month, the remaining photoreceptor nuclei in all three strains stain darkly (Figs. 3A–3D) making the morphological identification of apoptotic nuclei by LM difficult.

As the ONL thins, the ultrastructural changes in the photoreceptor layer are similar but not identical to those reported in other murine inherited retinal degenerations (Caley et al., 1972; Sanyal & Bal, 1973; Carter-Dawson et al., 1978; Blanks et al., 1982; Gouras & Tanabe, 2003). Surviving photoreceptors in the RBF and 4Bnr strains tilt such that their IS and OS are oriented at highly oblique angles to the outer limiting membrane (OLM) (Figs. 3F & 3H). Ectopic stacks or whorls of OS membranes frequently lie within the receptor IS (Figs. 2I & 3H) or in the apical perinuclear cytoplasm (data not shown). In the 4Bnr strain, OS frequently occur as thin, elongated stacks of membranes often folded back on themselves (Fig. 3H). Degenerating rod spherules are often vacuolized (Fig. 3G) as has been described in the *pcd* mutant mouse (Blanks et al., 1982); this is never seen in control mice of any age. As the photoreceptors die, processes of adjacent Müller cells overlap and fill in space. The apical cytoplasm of these Müller cells contains few organelles except occasional electron-dense vacuolar inclusions (Fig. 2I). Müller cells remain joined by the cell junctions of the OLM (Figs. 2G, 2I, 3F, & 3H), and their apical microvilli project into the subretinal space (SRS) (Figs. 2I, 3F, & 3H) towards an even thicker array of RPE apical microvilli (Figs. 3D, 3F, & 3H).

Developmental sequence: Postnatal weeks five to seventeen (P28 to P120)

At the beginning of the second month of development only the In-30 strain has photoreceptor IS and OS still recognizable by LM (Fig. 4A). By the end of the sixth week they together are 21–25 μm long and are still arranged rather typically, although cell bodies in the ONL are atypically angular in profile (data not shown). As mentioned above, the cell bodies of surviving photoreceptors are mostly pyknotic in appearance, making it difficult to identify those cells actually undergoing apoptosis, and/or to distinguish rods from cones using the accepted criteria in mice (Carter-Dawson & LaVail, 1979). Even so, in older animals where the ONL is a single, discontinuous layer of scattered photoreceptors (Figs. 4B, 4D, & 4E), both rods and cones are still present, since EM reveals both rod spherules and cone pedicles in the 4Bnr strain at P42 (Fig. 4F), and in the RBF strain at P55 (Fig. 4H). Despite the loss of most photoreceptors, the processes of the OPL neuropil appear remarkably normal. Not until P120, the latest stage examined, did the OPL neuropil in the In-30 strain appear degenerated.

With most photoreceptors gone, Müller cell processes fill the former ONL. We saw no evidence for the migration of Müller cell bodies into the ONL or the subretinal space, and only rarely did a Müller cell process grow into the former interphotoreceptor space, common events during the photoreceptor degeneration induced by retinal detachment (Erickson et al., 1983).

The array of RPE apical microvilli that is obvious early (Figs. 3D, 3F, & 3H) transforms later into a few tightly packed microvilli that run along this interface and form a honeycomb pattern when cross-sected (Figs. 4F, 4G, & 4H). Common to all strains, but easier to see in the pigmented In-30 specimens, are focal regions of RPE cell loss. In response, neighboring RPE cells spread out laterally (Figs. 3D, 4D, & 4F), often to the point that the remaining neural retina—often cells of the INL—fronts on Bruch's membrane with only thin strands of Müller cell cytoplasm interposed (Figs. 3D & 4G), if that (Figs. 4C & 4D). [At the other extreme, we infrequently encountered a second, interposed layer of RPE in the SRS (Fig. 3E).] We observed no obvious pattern to such RPE cell dropout except that it occurred regularly late in the degeneration. We saw few examples of apoptotic profiles in this monolayer (Figs. 1M & 5E) but often encountered vacuolized (Fig. 2C) and necrotic RPE cells (data not shown) especially in older animals. We attempted no quantification of RPE cell loss.

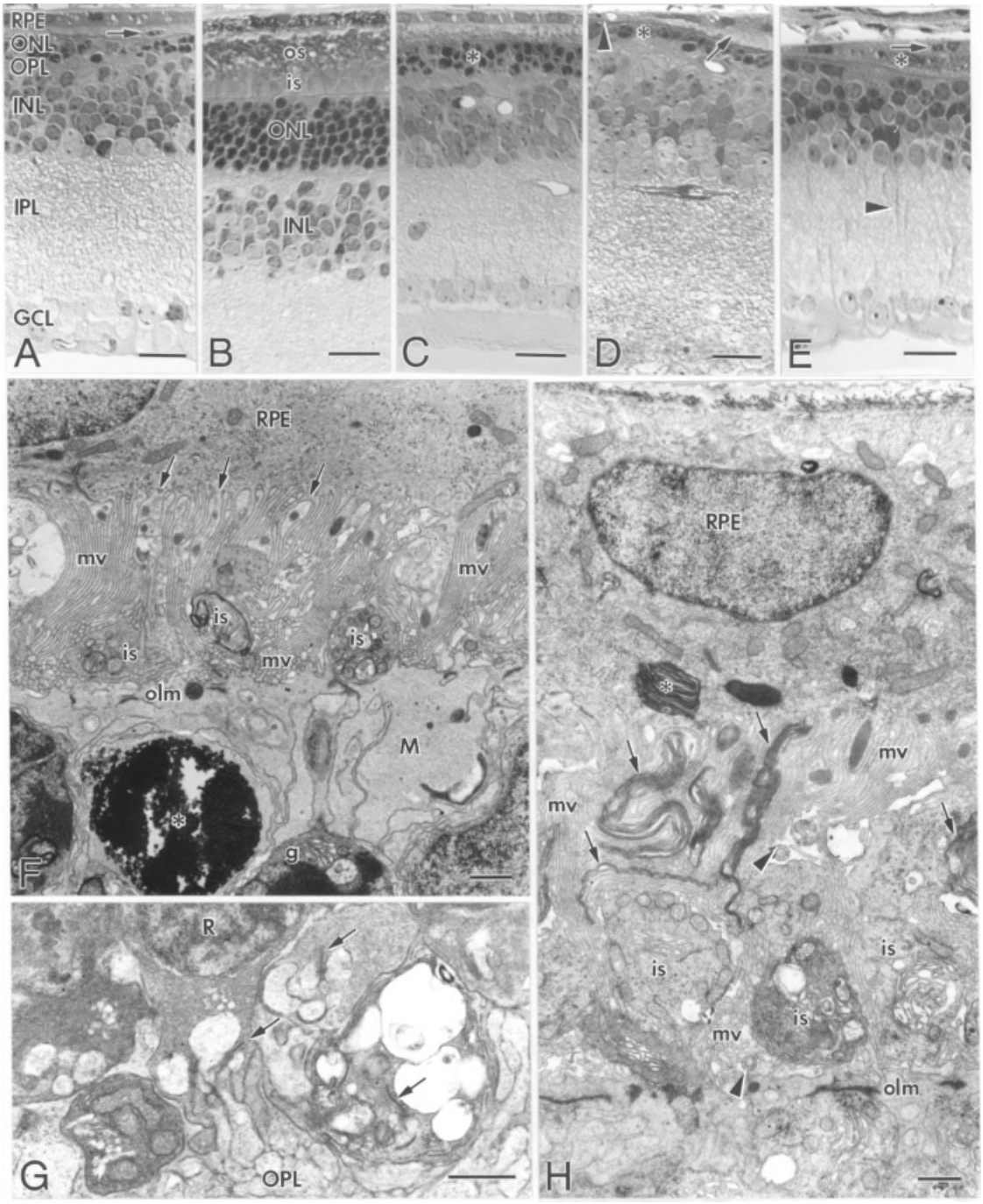

Fig. 3. A: LM of central retina, P24, 4Bnr strain. The OPL is discontinuous. Neither photoreceptor OS nor IS are evident in the subretinal space, though a presumed macrophage is (arrow). 425×. B: LM of central retina, P27, In-30 strain. IS and OS are identifiable though the latter appear scrambled. 425×. C: LM of central retina, P28, RBF strain. The ONL (*) has only 2–3 rows of photoreceptor cell bodies. Blood vessels are evident in the outer INL and IPL. 425×. D: LM of central retina, P28, 4Bnr strain. The thin ONL (*) underlies the RPE which is very thin in some areas (arrowhead), while adjacent regions appears thicker due to dense arrays of apical microvilli that fill the subretinal space (arrow). 425×. E: LM of midperipheral retina, P32, 4Bnr strain. A second layer of RPE (*) is interposed between the primary layer (arrow) and the neural retina. The ONL is discontinuous and the OPL is not apparent. Thick Müller cell processes rise through the IPL (arrowhead). 425×. F: EM of the retinal-RPE interface in a 3-week mouse, 4Bnr strain, which is dominated by interdigitating apical microvilli (mv) elaborated by both RPE and Müller cells. Arrows indicate where these villous processes arise from the RPE cytoplasm; some contain lysosomes. Three receptor IS projecting almost horizontally out of the plane of section, contain a few mitochondria and vacuoles of varying size. Müller cells extensively overlap at the OLM, their apical cytoplasm (M) largely lacks organelles. A remaining rod photoreceptor adjacent to an apoptotic profile (*) contains an ectopic, perinuclear Golgi body (g). 7000×. G: EM of a patch of six rod spherules fronting on the OPL in the retina of a P21 mouse, In-30 strain. The terminal at the lower right has collapsed and heavily vacuolized cytoplasm. R = rod nucleus; arrows = synaptic ribbons. 11,500×. H: EM of the RPE and outer retina of a 3-week mouse, 4Bnr strain. The subretinal space is crowded with apical microvilli (mv) from both the RPE and Müller cells, several photoreceptor IS, as well as thin, atypically elongated stacks of OS (arrows). A phagosome (*) lies in RPE cell apical cytoplasm; lysosomes occur in some apical processes. Arrowheads = cross sections of photoreceptor connecting cilia; olm = outer limiting membrane. 7250×. Scale bars: A–E = 20 μm; F–H = 1 μm.

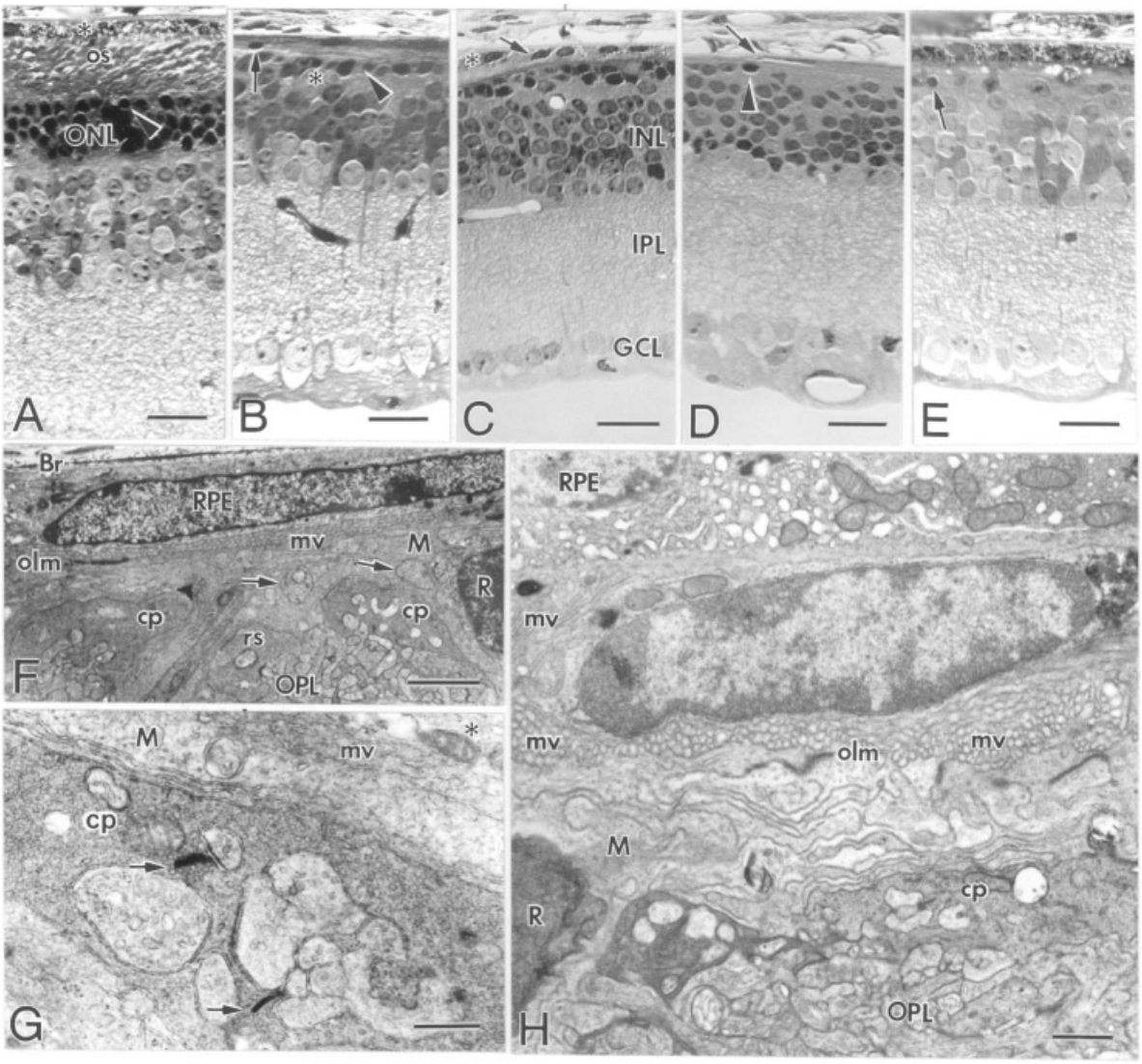

Fig. 4. A: LM of central retina, P45, In-30 strain. Receptor OS are still discernible beneath the RPE (*). Arrowhead = an apoptotic cell. 425×. B: LM of posterior retina, P54, RBF strain. The ONL is a monolayer (arrowhead); the ONL and OPL (*) are discontinuous. Arrow = probable macrophage. 425×. C: LM of midperipheral retina, P56, 4Bnr strain. The RPE monolayer (*) ends in a region where four macrophage-like cells (arrow) lie in subretinal space that apparently fronts directly on the choroid. 425×. D: LM of midperipheral retina, P76, RBF strain. An apoptotic photoreceptor cell (arrowhead) lies in the discontinuous ONL. The overlying RPE monolayer is thin and appears to end (arrow). 425×. E: LM of central retina, P100, In-30 strain. An apoptotic photoreceptor cell (arrow) lies in a discontinuous ONL. 425×. F: EM of the outer central retina, P42, 4Bnr strain. A thin and elongate nucleus lies in a flattened RPE cell. A narrow subretinal space contains microvilli (mv) seen in cross section. A single rod nucleus (R) comprises the ONL. A rod spherule (rs), two cone pedicles (cp), and the OPL neuropil lie close to the RPE-retinal interface. Arrows = cross sections of photoreceptor axons projecting out of the plane of section; M = Müller cell apical cytoplasm; Br = Bruch's membrane. 5100×. G: EM of the outer retina, P42, 4Bnr strain. The RPE (*) is greatly attenuated. A cone pedicle (cp) lies beneath a thin strip of Müller cell cytoplasm (M) that is separated from the RPE by a thin array of microvilli (mv). Arrows = synaptic ribbons. 19,500×. H: EM of the outer retina, P55, RBF strain. An interdigitating array of Müller cell apical processes (M) overlies the OPL neuropil and photoreceptor synaptic terminals, including a cone pedicle (cp). A macrophage-like cell in the subretinal space is surrounded on three sides by microvilli (mv). R = rod nucleus; olm = outer limiting membrane. 8700×. Scale bars: A–E = 20 μm; F = 2 μm; G = 0.5 μm; H = 1 μm.

Effects of the degeneration on the inner retina

The OPL neuropil begins to be discontinuous starting around the fourth postnatal week (Figs. 4B, 4D, 4E, & 4F). Measurements of INL thickness showed relatively little difference between the mutant strains and control retinas of the same age (see Fig. 8D; Tables 1–4). After the end of normal developmental apoptosis in this layer, we rarely saw TUNEL positive profiles here. There were no obvious changes in the IPL and GCL, so we did not quantitate their thickness across the time course of this study.

TUNEL and immunocytochemistry

The pattern of cells positive for TUNEL closely corresponds to the results obtained using standard morphological criteria for apop-

totic cells. Though only data from the 4Bnr strain is shown, the results, except for their timing, were similar in all three strains (see Tables 1–3). At P6 and P10, TUNEL-positive profiles were mostly restricted to the INL and GCL of the inner retina (Figs. 5A & 5B). Starting at P14 there is a rapid increase in the number of TUNEL-positive profiles within the ONL (Fig. 5C) that reaches a peak near P21 (Fig. 5D). Between these two time points, TUNEL-positive cells in the inner retina disappear. The loss of photoreceptors in the 4Bnr strain after P21 is especially rapid, and so at later time points TUNEL-labeled profiles are restricted to an increasingly narrow ONL, as shown for a P35 specimen (Fig. 5E). At this latter time point, occasional TUNEL-positive profiles occur in the RPE monolayer.

Except for fine points in timing, changes in rod opsin expression apply to all three strains. At P6, intense rod opsin labeling is restricted to the apical tips of the developing photoreceptors—representing the first indicator of OS development (Fig. 6A). Small, punctate profiles labeled in the RPE probably represent phagosomes (Fig. 6A). At P14, the OS have greatly lengthened and are intensely labeled (Fig. 6B). By P21 OS are still rod opsin-positive, but show significant signs of disruption. The thickness of the ONL is still comparable to that of the P14 specimen (Fig. 6C). By P56 the ONL is reduced to 2–3 rows of photoreceptor cell bodies and few anti-rod opsin labeled OS remain (Fig. 6D). Faint labeling by the rod opsin antibody of the plasma membrane around the photoreceptor cell bodies occurs at the same time as the OS develop (Fig. 6A), intensifies slightly as the OS mature (Figs. 6B & 6C), and remains in surviving photoreceptor cell bodies long after the OS have completely degenerated (P77, Fig. 6E).

At P6 and P14, anti-GFAP labeling was restricted to astrocytes at the internal limiting membrane (ILM) (Figs. 7A & 7B). At P21, when OS degeneration is underway, GFAP-positive Müller cells extend from the ILM through the inner retina, to the OLM (Fig. 7C). This Müller cell labeling appears more robust at P56 (Fig. 7D) and P77 (Fig. 7E), but the Müller cell radial processes never appear to thicken appreciably or to form glial scars on the retinal surfaces.

Discussion

While the *rd-3* mutant strains have the massive loss of photoreceptor cells in common with other retinal degenerations, there are also distinctive differences. Unlike the RPE cells of the RCS rat (Bok & Hall, 1971; Mullen & LaVail, 1976), based on our morphological observations, RPE cells of the *rd-3/rd-3* mouse are competent to phagocytose OS. Unlike the rod photoreceptors of the *Rds/Rds* mouse (Sanyal & Jansen, 1981), all three strains of the *rd-3* homozygotes clearly are able to assemble OS discs, although they are not all normal in either size or orientation. In considering the overall pattern of cell loss, the *rd-3/rd-3* degeneration shows no apparent preference for rods over cones or for center *versus* periphery and thus differs from the *rd/rd* mouse where rods are lost before cones (Carter-Dawson et al., 1978), from the *Rds/Rds* mouse (Sanyal et al., 1980) or *mnd/mnd* mouse (Chang et al., 1994; Guarneri et al., 2004) where peripheral photoreceptors are lost faster than central ones, and from the $mitf^{vit}$ mouse where the reverse is true (Smith, 1995). Finally, *rd-3* and all of the other retinal degenerations listed above are pan-retinal in their expression unlike that in the $Crb1^{rd8}$ degeneration where only the inferior nasal quadrant of the retina is affected (Mehalow et al., 2003).

The TUNEL data show that photoreceptors die by apoptosis in this mutation as in every other retinal degeneration described to date, whether inherited (Chang et al., 1993*b*; Portera-Cailliau et al., 1994; Tso et al., 1994; Smith et al., 1995; Ikeda et al., 1999; Guarneri et al., 2004), or induced (Shahinfar et al., 1991; Cook et al., 1995).

In the murine retinal degenerations described above, the developmental stage at which the effect of the mutant genes becomes expressed varies widely. The earlier the onset, as in *rd*, the less mature the OS will be as photoreceptor cells begin to die *en masse*. OS begin to form in the *rd* retina (Caley et al., 1972; Sanyal & Bal, 1973), but never develop beyond short, abnormal structures. In degenerations with late apoptotic onset, such as in *mnd* (Messer et al., 1993; Chang et al., 1994; Guarneri et al., 2004) $mitf^{vit}$ (Smith, 1992; Sidman et al., 1996; Bora et al., 1999), or $Rpe65^{rd12}$ (Pang et al., 2005), photoreceptor OS are usually mature, though sometimes shorter than normal as the die-off commences. The onset of apoptosis in the *rd-3/rd-3* mouse is intermediate between these examples. However, there are important differences among the three strains: the albino 4Bnr and RBF strains begin mass apoptosis earlier than the pigmented In-30 strain (see Fig. 8A), and the OS of the latter achieve the most mature configuration of all three strains, although none reach a fully mature phenotype.

In most of the inherited retinal degenerations including *rd-3*, the RPE and macrophages play active roles in phagocytosing debris from dying photoreceptors (Finnemann & Rodriguez-Boulan, 1999; Hisatomi et al., 2003). The RPE also alters the morphology of its numerous apical processes becoming radically different from those in normal retina, and Müller cell processes fill in for dying photoreceptors while also becoming strongly immunoreactive for intermediate filament proteins such as GFAP and vimentin.

As the remaining photoreceptors in the *rd-3* retinas dwindle to an incomplete monolayer, the RPE cells increasingly contain clumped debris and/or become heavily vacuolated. Their apical microvilli become greatly reduced in size and number. Some RPE cells appear necrotic. Profiles of dying RPE cells are rare, which may not be surprising given the rapidity of the apoptotic process and the small number of cells that lie in a single histological section spanning the RPE monolayer. Late in the degeneration when few photoreceptor cell bodies are present, RPE cell death becomes more obvious and neighboring cells flatten and thin dramatically as if they fill in the gaps. This focal pattern of RPE cell dropout correlates with the mottled appearance of the fundus reported at 4–6 months postnatally in the pigmented In-30 strain (Heckenlively et al., 1993*a*; Hawes et al., 1999; Chang et al., 2002). Such patterns of hypopigmentation, due to a variety of causes including but not limited to RPE cell dropout, have been seen in fundus photographs of most of the known murine inherited retinal degenerations (Hawes et al., 1999; Chang et al., 2002; Mehalow et al., 2003; Pang et al., 2005). As we have reported here, several studies correlate areas of RPE cell thinning with the apposing and localized loss of photoreceptor cell bodies comprising the ONL (Caley et al., 1972; Sanyal & Bal, 1973; Sanyal et al., 1980; LaVail et al., 1982, 1993; Blanks et al., 1982; Messer et al., 1993). As in other photoreceptor degenerations, Müller cells fill in space left by these dying photoreceptors. Though immunocytochemistry shows that there is some upregulation of GFAP in these cells, as has been seen in other retinal degenerations (Eisenfeld et al., 1984; Lewis et al., 1994), we found no evidence of extensive Müller cell hypertrophy in the inner retina nor did these cells grow beyond the OLM to form membranes or scars in the subretinal space. By comparison, 3 days of retinal detachment in cats or rabbits is sufficient to promote significant hypertrophy of Müller cells in all retinal layers and to induce their growth onto the

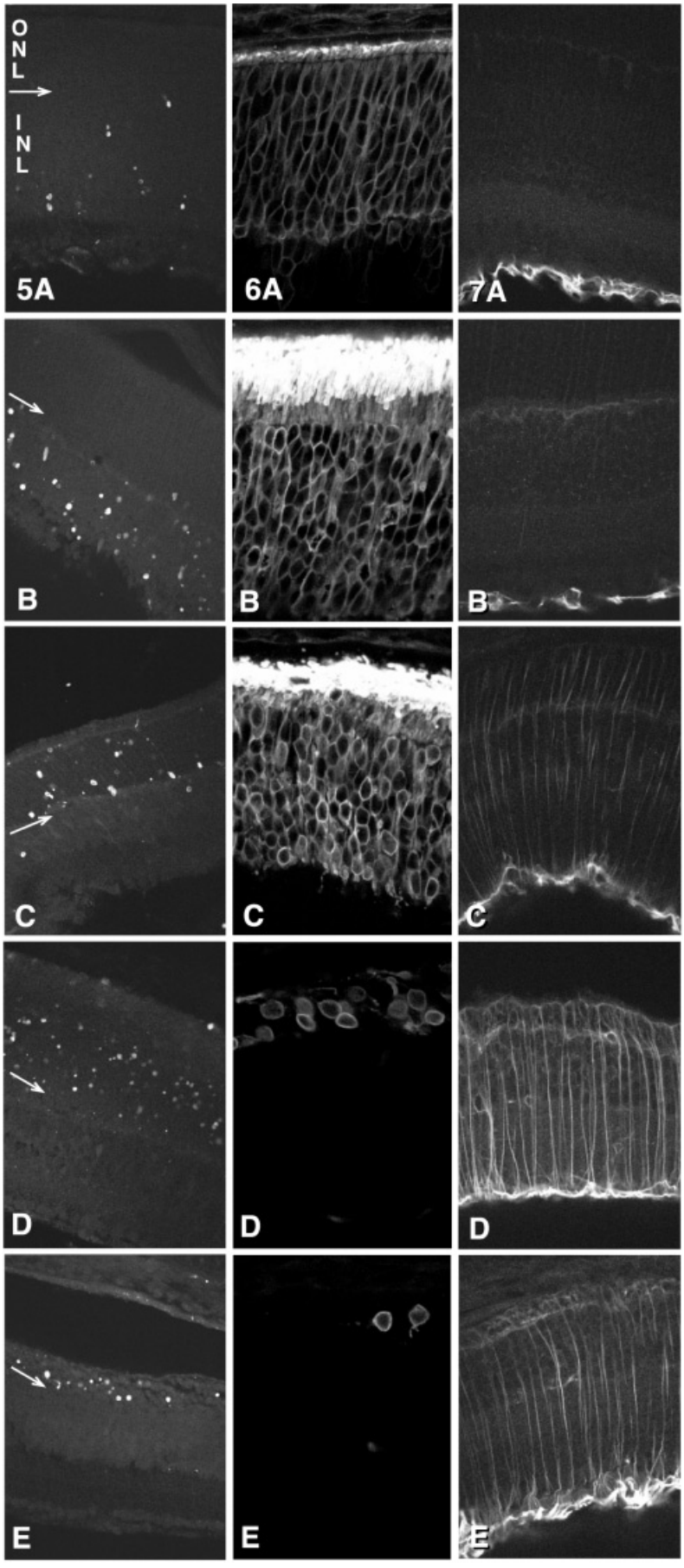

Fig. 5–7. Confocal micrographs of the developing central retina of the 4BnR strain of the *rd-3* afflicted mice. (5A–5E) Retinal sections labeled using a modified version of the TUNEL technique. The arrow in all figures points to the OPL. 5A: At P6, TUNEL-labeled cells are confined to the inner retina among amacrine and ganglion cells. 5B: At P10, there is an increase in apoptotic profiles though they are still restricted to the inner retinal layers. 5C: At P14, TUNEL-labeled cells appear in the ONL while few are seen in the inner retina. 5D: At P21, the number of apoptotic profiles in the ONL reaches a maximum. 5E: By P35, the ONL has been reduced to a few rows of photoreceptors many of which are undergoing apoptosis. TUNEL-positive profiles also appear in the RPE monolayer. (6A–6E) Central retina immunolabeled with an antibody to rod opsin. 6A: At P6, rod opsin is localized to the short IS and OS and faintly to the plasma membrane around the cell bodies in the ONL. 6B: By P14, the IS and OS have lengthened greatly and labeling around the cell bodies has intensified. 6C: At P21, both the IS and OS are somewhat shorter and appear increasingly disrupted. Rod opsin labeling of the plasma membrane around the photoreceptor cell bodies remains prominent. 6D: By P56, the ONL contains only a few rows of photoreceptor cell bodies whose plasma membranes are faintly labeled with the rod opsin antibody. 6E: By P77, photoreceptors lack both OS and IS yet faint rod opsin labeling persists around the few surviving cell bodies. (7A–7E) Retinal sections immunolabeled with antibodies to glial fibrillary acidic protein (GFAP), a marker for glial intermediate filaments. 7A: At P6, GFAP labeling is most robust in the retinal astrocytes and Müller cell endfeet fronting on the inner limiting membrane (ILM). 7B: At P14, a similar pattern of GFAP labeling persists along with faint labeling of presumed HCs. 7C: At P21, GFAP-positive radial fibers extend from the ILM to the OLM. 7D: At P56, the radial fibers label even more robustly. Intense endfoot/astrocyte labeling persists as does faint labeling of HCs. 7E: Even as late as P77 when the ONL is reduced to a discontinuous monolayer, Müller cell radial fibers show no signs of hypertrophy or scar formation.

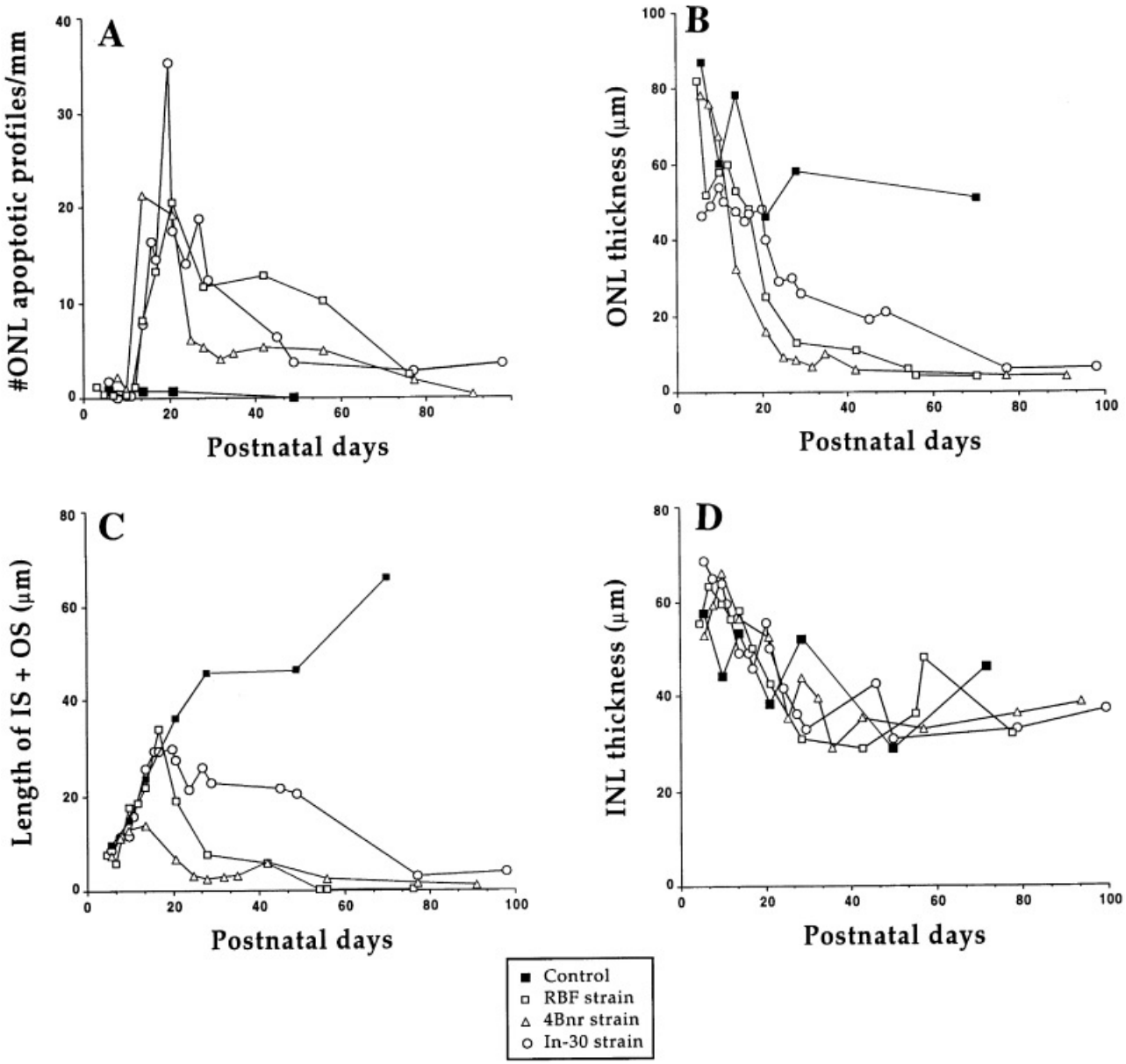

Fig. 8. Graphs showing developmental changes in the retinas of normal and *rd-3/rd-3* mice. Most data points represent a single animal (see Tables 1–4); those where $n > 1$ are the average of all specimens. Filled squares: controls; open squares: RBF strain; open triangles: 4Bnr strain; open circles: In-30 strain. A: A plot of the number of apoptotic profiles per millimeter of retina versus postnatal day reveals that apoptosis in the ONL peaks around P20 for all strains while the control mice have virtually no apoptotic cells in that layer. The 4Bnr strain appears to have the earliest apoptotic onset and a burst of cell death before the rate of apoptosis levels off. Photoreceptor apoptosis appears to be completed first in the RBF strain. B: A plot of ONL thickness *versus* postnatal day shows that while all animals experience an early decrease in this layer's thickness, the ONL of the control animals level off after 20 days. This same layer in all three mutant strains rapidly thins due to the resident photoreceptors dying. The 4Bnr strain appears to have the most accelerated thinning; the In-30 strain the slowest. C: A plot of the combined lengths of inner (IS) and outer segments (OS) *versus* postnatal day shows that these distal structures form at about the time and rate in all animals. As photoreceptors die, they lose these outer structures and the graph shows that those of the 4Bnr strain are the shortest as mass apoptosis sets in; those of the In-30 strain persist the longest. None of the strains has IS and OS that attain normal adult length. D: A plot of INL thickness *versus* postnatal day demonstrates that after an early period of histogenetic thinning, all three strains have an INL layer essentially the same thickness as the controls despite the total loss of the ONL.

photoreceptor surface (Erickson et al., 1983; Lewis et al., 1994). This provides an interesting comparison of Müller cell reactivity, because in the feline detachment model, Müller cell hypertrophy is very robust, especially considering that the actual loss of photoreceptors is much less than in the numerous inherited degenerations discussed here. In addition, as seen in the later stages of the *rd-3* degeneration, changes spread beyond the ONL to the OPL. As early as P24, the OPL appears disorganized due to the loss of horizontal and bipolar cell processes presumably in response to the death of photoreceptors. The pruning of second-order neurons

from the OPL has also been reported in the *rd* degeneration (Strettoi & Pignatelli, 2000; Strettoi et al., 2003; Gouras & Tanabe, 2003) which provides another point of contrast to the responses after retinal detachment where rod bipolar cells and horizontal cells rapidly sprout neurites that grow into the ONL and even into the subretinal space (Lewis et al., 1998).

Conclusions

In this study, we focused on one of the criteria set forth by LaVail (1981) for characterizing inherited retinal degeneration: describing the mutation's phenotype by defining the time course of cytopathological events. In the *rd-3* mutation, photoreceptor cells appear to be structurally normal until outer segment differentiation is well underway. In later stages, the expression of rod opsin in the plasma membrane surrounding the cell bodies (Fariss et al., 1997) remains apparently for as long as the cell survives, well after the OS degeneration is complete. Although we demonstrated that *rd-3* photoreceptors die *via* apoptosis, the identity of the gene causing the cells to degenerate and eventually die remains unknown (see Danciger et al., 1999). Just because this mutation results in the loss of photoreceptors does not prove that they, in fact, are the target site of the genetic lesion. While this is true in many inherited retinal degenerations (the *rd* mouse, for example; Farber et al., 1994; Lolley et al., 1994), it is not true in the RCS rat (Mullen & LaVail, 1976).

The fact that we have been able to demonstrate significant differences in both the morphology and time course of the degeneration between the three strains described here is a clear indication of the importance of the overall genetic background of an organism on the expression of a specific genetic trait. Many genetic differences among the three strains could affect the course of degeneration caused by the *rd-3* mutation. One obvious possibility is the albinism of the RBF and 4Bnr strains that may make them more susceptible to photic damage than their pigmented counterpart (LaVail & Battelle, 1975). Albinism is not likely to provide the full mechanism, however, since even here, we have documented subtle differences between the two albino strains, and more fundamentally, because LaVail and colleagues (1987) already have demonstrated differences in susceptibility to light damage among albino strains of mice.

The ability of secondary genes or background to affect the severity of specific retinal inherited degenerations is now appreciated for a number of these allelic variations (Heckenlively et al., 1993*a*,*b*; Hawes et al., 1999; Messer et al., 1999; Mehalow et al., 2003; Guarneri et al., 2004). This is also recognized as an important source of variance in families with respect to disease phenotype. Thus, further study of differences between the three strains of mice carrying the *rd-3* mutation may yield important clues to understanding such variation in the human diseases. Moreover, study of the *rd-3* mutation might also lead to clues for therapies to prolong photoreceptor survival in human disease.

Acknowledgments

The authors wish to acknowledge the contributions of Drs. Cathy Bowes-Rickman, Jan Danciger, Michael Madtes, Geoff Lewis, Brian Matsumoto, as well as Bo Chang, Maura Jess, Justin Dice, Karen Guenther, Orianna Cavallero, Rick Hussey, Garrick Lo, and Richard Rothstein. This research was supported by NIH grants EY07758 to J.R. Heckenlively, EY02651 to D.B. Farber, EY00888 to S.K. Fisher, and a grant from the Foundation Fighting Blindness to D.B. Farber, who is also the recipient of a Research to Prevent Blindness Senior Scientist Ivnestigator's Award.

References

Blanks, J.C., Mullen, R.J. & LaVail, M.M. (1982). Retinal degeneration in the *pcd* cerebellar mutant mouse. II. Electron microscopic analysis. *Journal of Comparative Neurology* **212**, 231–246.

Bok, D. & Hall, M. (1971). The role of the pigment epithelium in the etiology of inherited retinal dystrophy in the rat. *Journal of Cell Biology* **49**, 664–682.

Bora, N., Defoe, D. & Smith, S.B. (1999). Evidence of decreased adhesion between the neural retina and retinal pigmented epithelium of the Mitf^{vit} (vitiligo) mutant mouse. *Cell and Tissue Research* **295**, 65–75.

Caley, D.W., Johnson, C. & Liebelt, R.A. (1972). The postnatal development of the retina in the normal and rodless CBA mouse: A light and electron microscopic study. *American Journal of Anatomy* **133**, 179–212.

Carter-Dawson, L.D. & LaVail, M.M. (1979). Rods and cones in the mouse retina. I. Structural analysis using light and electron microscopy. *Journal of Comparative Neurology* **188**, 245–262.

Carter-Dawson, L.D., LaVail, M.M. & Sidman, R.L. (1978). Differential effect of the *rd* mutation on rods and cones in the mouse retina. *Investigative Ophthalmology and Visual Science* **17**, 489–498.

Chang, B., Bronson, R.T., Hawes, N.L., Roderick, T.H., Peng, C., Hageman, G.S. & Heckenlively, J.R. (1994). Retinal degeneration in motor neuron degeneration: A mouse model of ceroid lipofuscinosis. *Investigative Ophthalmology and Visual Science* **35**, 1071–1076.

Chang, B., Hawes, N.L., Hurd, R.E., Davisson, M.T., Nusinowitz, S. & Heckenlively, J.R. (2002). Retinal degeneration mutants in the mouse. *Vision Research* **42**, 517–525.

Chang, B., Heckenlively, J.R., Hawes, N.L. & Roderick, T.H. (1993*a*). New mouse primary retinal degeneration (*rd-3*) linked to chromosome 1 distal to Akp-1. *Genomics* **16**, 45–49.

Chang, G.-Q., Hao, Y. & Wong, F. (1993*b*). Apoptosis: final common pathway of photoreceptor death in *rd*, *rds*, and rhodopsin mutant mice. *Neuron* **11**, 595–605.

Cook, B., Lewis, G.P., Fisher, S.K. & Adler, R. (1995). Apoptotic photoreceptor degeneration in experimental retinal detachment. *Investigative Ophthalmology and Visual Science* **36**, 990–996.

Danciger, J.S., Danciger, M., Nusinowitz, S., Rickabaugh, T. & Farber, D.B. (1999). Genetic and physical maps of the mouse rd3 locus, exclusion of the ortholog of USH2A. *Mammalian Genome* **10**, 657–661.

Eisenfeld, A.J., Bunt-Milam, A.H. & Sarthy, P.V. (1984). Müller cell expression of glial fibrillary acidic protein after genetic and experimental photoreceptor degeneration in the rat retina. *Investigative Ophthalmology and Visual Science* **25**, 1321–1328.

Erickson, P.A., Fisher, S.K., Anderson, D.H., Stern, W.H. & Borgula, G.A. (1983). Retinal detachment in the cat: The outer nuclear layer and outer plexiform layers. *Investigative Ophthalmology and Visual Science* **24**, 927–942.

Farber, D.B., Flannery, J.G. & Bowes-Rickman, C. (1994). The *rd* mouse story: seventy years of research on an animal model of inherited retinal degeneration. *Progress in Retinal Research* **13**, 31–64.

Fariss, R.N., Molday, R.S., Fisher, S.K. & Matsumoto, B. (1997). Evidence from normal and degenerating photoreceptors that two outer segment integral membrane proteins have separate transport pathways. *Journal of Comparative Neurology* **387**, 148–156.

Fariss, R.N., Linberg, K.A., Lo, G.J., Heckenlively, J.R., Peng, C. & Fisher, S.K. (1994). Retinal degeneration in the *rd-3* mouse leads to changes in the immunolocalization of Müller cell and photoreceptor proteins. *Investigative Ophthalmology and Visual Science* **35**, (ARVO Supplement) 1610.

Finnemann, S.C. & Rodriguez-Boulan, E. (1999). Macrophage and retinal pigment epithelium phagocytosis: Apoptotic cells and photoreceptors compete for $\alpha v\beta 3$ and $\alpha v\beta 5$ integrins, and protein kinase C regulates $\alpha v\beta 5$ binding and cytoskeletal linkage. *Journal of Experimental Medicine* **190**, 861–874.

Fisher, S.K., Anderson, D.H., Erickson, P.A., Guérin, C.J., Lewis, G.P. & Linberg, K.A. (1993). Light and electron microscopy of vertebrate photoreceptors including a technique for electron microscopic autoradiography. *Methods in Neuroscience* **15**, 3–36.

Gavrieli, Y., Sherman, Y. & Ben-Sasson, S.A. (1992). Identification of programmed cell death *in situ via* specific labeling of nuclear DNA fragmentation. *Journal of Cell Biology* **119**, 493–501.

Gouras, P. & Tanabe, T. (2003). Ultrastructure of adult rd mouse retina. *Graefe's Archive for Clinical and Experimental Ophthalmology* **241**, 410–417.

Guarneri, R., Russo, D., Cascio, C., D'Agostino, S., Galizzi, G., Bigini, P., Mennini, T. & Guarneri, P. (2004). Retinal oxidation, apoptosis and age- and sex-differences in the mnd mutant mouse, a model of neuronal ceroid lipofuscinosis. *Brain Research* **1014**, 209–220.

Hawes, N.L., Smith, R.S., Chang, B., Davisson, M., Heckenlively, J.R. & John, S.W.M. (1999). Mouse fundus photography and angiography: A catalogue of normal and mutant phenotypes. *Molecular Vision* **5**, 22.

Hawes, N.L., Chang, B., Hageman, G.S., Nusinowitz, S., Nishina, P.M., Schneider, B.S., Smith, R.S., Roderick, T.H. & Davisson, M.T. (2000). Retinal degeneration 6 (*rd6*): A new model for human retinitis punctata albescens. *Investigative Ophthalmology and Visual Science* **41**, 3149–3157.

Heckenlively, J.R., Chang, B., Hawes, N.L., Peng, C. & Roderick, T.H. (1993*a*). Variable expressivity of *rd-3* dependent on strain. *Investigative Ophthalmology and Visual Science* **34** (ARVO Supplement) 741.

Heckenlively, J.R., Chang, B., Peng, C., Hawes, N.L. & Roderick, T.H. (1993*b*). Variable expressivity of *rd-3* retinal degeneration dependent on background strain. In *Retinal Degeneration*, ed. Hollyfield, J.G., Anderson, R.E. & LaVail, M.M., pp. 273–280, New York: Plenum Press.

Heckenlively, J.R., Chang, B., Erway, L.C., Peng, C., Hawes, N.L., Hageman, G.S. & Roderick, T.H. (1995). Mouse model for Usher syndrome: Linkage mapping suggests homology to Usher type I reported at human chromosome 11p15. *Proceedings of the National Academy of Sciences of the U.S.A.* **92**, 11100–11104.

Hisatomi, T., Sakamoto, T., Sonoda, K., Tsutsumi, C., Qiao, H., Enaida, H., Yamanaka, I., Kubota, T., Ishibashi, T., Kura, S., Susin, S.A. & Kroemer, G. (2003). Clearance of apoptotic photoreceptors: Elimination of apoptotic debris into the subretinal space and macrophage-mediated phagocytosis via phosphatidylserine receptor and integrin $\alpha v\beta 3$. *American Journal of Pathology* **162**, 1869–1879.

Ikeda, S., He, W., Ikeda, A., Naggert, J.K., North, M.A. & Nishina, P.M. (1999). Cell-specific expression of Tubby gene family members (*tub, Tulp1, 2*, and *3*) in the retina. *Investigative Ophthalmology and Visual Science* **40**, 2706–2712.

Lamoreux, M.L., Boissy, R.E., Womack, J.E. & Nordlund, J.J. (1992). The vit gene maps to the mi (microphthalmia) locus of the laboratory mouse. *Journal of Heredity* **83**, 435–439.

LaVail, M.M. (1981). Analysis of neurological mutants with inherited retinal degeneration. *Investigative Ophthalmology and Visual Science* **21**, 638–657.

LaVail, M.M. & Battelle, B.-A. (1975). Influence of eye pigmentation and light deprivation on inherited retinal dystrophy in the rat. *Experimental Eye Research* **21**, 167–192.

LaVail, M.M., Blanks, J.C. & Mullen, R.J. (1982). Retinal degeneration in the *pcd* cerebellar mutant mouse. I. Light microscopic and autoradiographic analysis. *Journal of Comparative Neurology* **212**, 217–230.

LaVail, M.M., Gorrin, G.M. & Repaci, M.A. (1987). Strain differences in sensitivity to light-induced photoreceptor degeneration in albino mice. *Current Eye Research* **6**, 825–834.

LaVail, M.M., White, M.P., Gorrin, G.M., Yasumura, D., Porrello, K.V. & Mullen, R.J. (1993). Retinal degeneration in the nervous mutant mouse. I. Light microscopic cytopathology and changes in the interphotoreceptor matrix. *Journal of Comparative Neurology* **333**, 168–181.

Lewis, G.P., Guérin, C.J., Anderson, D.H., Matsumoto, B. & Fisher, S.K. (1994). Rapid changes in the expression of glial cell proteins caused by experimental retinal detachment. *American Journal of Ophthalmology* **118**, 368–376.

Lewis, G.P., Linberg, K.A. & Fisher, S.K. (1998). Neurite outgrowth from bipolar and horizontal cells after experimental retinal detachment. *Investigative Ophthalmology and Visual Science* **39**, 424–434.

Linberg, K.A., Fariss, R.N., Heckenlively, J.R., Peng, C., Bowes, C., Farber, D.B. & Fisher, S.K. (1994). Structural changes in the developing retina of the *rd-3* mouse. *Investigative Ophthalmology and Visual Science* **35** (ARVO Supplement) 1610.

Lolley, R.N., Rong, H. & Craft, C.M. (1994). Linkage of photoreceptor degeneration by apoptosis with inherited defect in phototransduction. *Investigative Ophthalmology and Visual Science* **35**, 358–362.

Matsumoto, B. & Hale, I.L. (1993). Preparation of retinas for studying photoreceptors with confocal microscopy. In *Methods in Neuroscience*, Vol. 15, ed. Hargrave, P.C., pp. 54–71, San Diego, California: Academic Press.

Mehalow, A.K., Kameya, S., Smith, R.S., Hawes, N.L., Denegre, J.M., Young, J.A., Bechtold, L., Haider, N.B., Tepass, U., Heckenlively, J.R., Chang, B., Naggert, J.K. & Nishina, P.M. (2003). CRB1 is essential for external limiting membrane integrity and photoreceptor morphogenesis in the mammalian retina. *Human Molecular Genetics* **12**, 2179–2189.

Messer, A., Plummer, J., Wong, V. & LaVail, M.M. (1993). Retinal degeneration in motor neuron degeneration (*mnd*) mutant mice. *Experimental Eye Research* **57**, 637–641.

Messer, A., Manley, K. & Plummer, J.A. (1999). An early-onset congenic strain of the motor neuron degeneration (MND) mouse. *Molecular Genetics and Metabolism* **66**, 393–397.

Mullen, R.J. & LaVail, M.M. (1975). Two new types of retinal degeneration in cerebellar mutant mice. *Nature* **258**, 528–530.

Mullen, R.J. & LaVail, M.M. (1976). Inherited retinal dystrophy: Primary defect in pigment epithelium determined with experimental rat chimeras. *Science* **192**, 799–801.

Nusinowitz, S., Peng, C. & Heckenlively, J.R. (1997). Rod and cone electroretinograms (ERGs) in the *rd-3* mouse model of retinal degeneration. *Investigative Ophthalmology and Visual Science* **38**, (ARVO Supplement) S886.

Olney, J.W. (1968). An electron microscopic study of synapse formation, receptor outer segment development, and other aspects of developing mouse retina. *Investigative Ophthalmology* **7**, 250–268.

Pang, J., Chang, B., Hawes, N.L., Hurd, R.E., Davisson, M.T., Li, J., Noorwez, S.M., Malhotra, R., McDowell, J.H., Kaushal, S., Hauswirth, W.W., Nusinowitz, S., Thompson, D.A. & Heckenlively, J.R. (2005). Retinal degeneration 12 (*rd12*): A new, spontaneously arising mouse model for human Leber congenital amaurosis (LCA). *Molecular Vision* **11**, 152–162.

Portera-Cailliau, C., Sung, C.H., Nathans, J. & Adler, R. (1994). Apoptotic photoreceptor cell death in mouse models of retinitis pigmentosa. *Proceedings of the National Academy of Sciences of the U.S.A.* **91**, 974–978.

Roderick, T.H., Chang, B., Hawes, N.L. & Heckenlively, J.P. (1995). New retinal degenerations in the mouse. In *Degenerative Diseases of the Retina*, ed. Anderson, R.E., LaVail, M.M. & Hollyfield, J.G., pp. 77–85. New York: Plenum Press.

Sanyal, S. & Bal, A.K. (1973). Comparative light and electron microscopic study of retinal histogenesis in normal and *rd* mutant mice. *Zeitschrift für Anatomie und Entwicklungsgeschichte* **142**, 219–238.

Sanyal, S. & Jansen, H.G. (1981). Absence of receptor outer segments in the retina of *rds* mutant mice. *Neuroscience Letters* **21**, 23–26.

Sanyal, S., de Ruiter, A. & Hawkins, R.K. (1980). Development and degeneration of retina in *rds* mutant mice: Light microscopy. *Journal of Comparative Neurology* **194**, 193–207.

Shahinfar, S., Edward, D.P. & Tso, M.O.M. (1991). A pathologic study of photoreceptor cell death in retinal photic injury. *Current Eye Research* **10**, 47–59.

Sidman, R.D., Kosaras, B. & Tang, M. (1996). Pigment epithelial and retinal phenotypes in the vitiligo, mi^{vit}, mutant mouse. *Investigative Ophthalmology and Visual Science* **37**, 1097–1115.

Smith, S.B. (1992). C57BL/6J-*vit/vit* mouse model of retinal degeneration: Light microscopic analysis and evaluation of rhodopsin levels. *Experimental Eye Research* **55**, 903–910.

Smith, S.B. (1995). Evidence of a difference in photoreceptor cell loss in the peripheral versus posterior regions of the vitiligo (C57BL/6J-mi^{vit}/mi^{vit}) mouse retina. *Experimental Eye Research* **60**, 333–336.

Smith, S.B., Bora, N., McCool, D., Kutty, G., Wong, P., Kutty, R.K. & Wiggert, B. (1995). Photoreceptor cells in the vitiligo mouse die by apoptosis. TRPM-2/clusterin expression is increased in the neural retina and in the retinal pigment epithelium. *Investigative Ophthalmology and Visual Science* **36**, 2193–2201.

Strettoi, E. & Pignatelli, V. (2000). Modifications of retinal neurons in a mouse model of retinitis pigmentosa. *Proceedings of the National Academy of Sciences of the U.S.A.* **97**, 11020–11025.

Strettoi, E., Pignatelli, V., Rossi, C., Porciatti, V. & Falsini, B. (2003). Remodeling of second-order neurons in the retina of rd/rd mutant mice. *Vision Research* **43**, 867–877.

Tso, M.O.M., Zhang, C., Abler, A.S., Chang, C-J., Wong, F., Chang, G.-Q. & Lam, T.T. (1994). Apoptosis leads to photoreceptor degeneration in inherited retinal dystrophy of RCS rats. *Investigative Ophthalmology and Visual Science* **35**, 2693–2699.

Young, R.W. (1984). Cell death during differentiation of the retina in the mouse. *Journal of Comparative Neurology* **229**, 362–373.